

Membrane-Interaction Quantitative Structure–Activity Relationship (MI-QSAR) Analyses of Skin Penetration Enhancers

Tao Zheng,[†] A. J. Hopfinger,^{‡,§} Emilio X. Esposito,[‡] Jianzhong Liu,^{‡,§} and Yufeng J. Tseng^{*,‡,||}

New Technology Department, Global Research & Development, Avon Products, Inc., 1 Avon Place, Suffern, New York 10901-5605, The Chem21 Group, Inc., 1780 Wilson Drive, Lake Forest, Illinois 60045, College of Pharmacy, MSC09 5360, 1 University of New Mexico, Albuquerque, New Mexico 87131-0001, and Graduate Institute of Biomedical Electronics and Bioinformatics, Department of Computer Science and Information Engineering, National Taiwan University, No. 1 Sec. 4, Roosevelt Road, Taipei, Taiwan 106

Received January 22, 2008

Membrane-interaction quantitative structure–activity relationship (MI-QSAR) models for two skin penetration enhancer data sets of 61 and 42 compounds were constructed and compared to QSAR models constructed for the same two data sets using only classic intramolecular QSAR descriptors. These two data sets involve skin penetration enhancement of hydrocortisone and hydrocortisone acetate, and the enhancers are generally similar in structure to lipids and surfactants. A new MI-QSAR descriptor, the difference in the integrated cylindrical distribution functions over the phospholipid monolayer model, in and out of the presence of the skin penetration enhancer, $\Delta\sum h(r)$, was developed. This descriptor is dominant in the optimized MI-QSAR models of both training sets studied and greatly reduces the size and complexity of the MI-QSAR models as compared to those QSAR models developed using the classic intramolecular descriptors. The MI-QSAR models indicate that good penetration enhancers make bigger “holes” in the monolayer and are less aqueous-soluble, so as to preferentially enter the monolayer, than are poor penetration enhancers. The skin penetration enhancer thus alters the structure and organization of the monolayer. This space and time alteration in the structure and dynamics of the membrane monolayer is captured by $\Delta\sum h(r)$ and is simplistically referred to as “holes” in the monolayer. The MI-QSAR models explain 70–80% of the variance in skin penetration enhancement across each of the two training sets and are stable predictive models using accepted diagnostic measures of robustness and predictivity.

INTRODUCTION

In a previous paper,¹ a combination of classic and 4D-fingerprint² *intramolecular* quantitative structure–activity relationship (QSAR) descriptors was used to build skin penetration enhancer QSAR models. Four distinct data sets were modeled in which the polarity and size of the enhancer was varied as well as the size and polarity of the reference penetrant. The resultant QSAR models for each data set are different from one another and suggest that different mechanisms of enhanced skin transport are at play as a function of both size and polarity of the enhancer and the penetrant. The differences in the QSAR models and, correspondingly, in mechanisms of transport appear to be largest between polar and nonpolar penetrants.

In this current study, we have expanded the trial descriptor set used to build skin penetration enhancer QSAR models to both refine the current models and seek a better understanding of the mechanisms of enhanced transport. A limited form of structure-based QSAR analysis, called membrane-interaction QSAR, MI-QSAR, analysis² has been carried out in this study. MI-QSAR analysis models the transport of an

organic compound through a phospholipid monolayer, or bilayer, assembly using molecular dynamics simulation, MDS.³ The simulation properties and features determined from the MDS trajectories are included as members of the QSAR descriptor pool used in building the QSAR models. As such, the majority of descriptors from these MDS studies are *intermolecular* descriptors describing interactions between the skin penetration enhancer, in this case, and phospholipids composing the model mono- or bilayer assembly.

Some experimental studies of penetration enhancement have measured the lipophilicity (nonpolarity) of enhancers and also have investigated the corresponding relationships between enhancer nonpolarity and penetration enhancement potency.^{4,5} There is limited evidence to support the view that a common set of physicochemical properties governs the penetration enhancement of nonpolar drugs that are different from those of polar drugs.⁶

The design and implementation of penetration enhancers to facilitate the transport of compounds of limited percutaneous absorption is of high interest for delivery systems in both the cosmetic and pharmaceutical industries. The stratum corneum (SC) is known to be the rate-limiting barrier in skin for the percutaneous absorption of drugs and other organics. The SC consists of the remains of dead cells surrounded by multilamellar lipid bilayer membranes. Small hydrophobic or nonpolar molecules can partition into the SC and then

* Corresponding author voice: 886-2-3366-4888 # 529; Fax: 886-2-23628167; e-mail: yjtseng@csie.ntu.edu.tw.

[†] Avon Products.

[‡] The Chem21 Group, Inc.

[§] University of New Mexico.

^{||} National Taiwan University.

diffuse across the lipid bilayer membranes, which is referred to as the intercellular route. However, hydrophilic (polar) molecules can best penetrate the SC through the transcellular route or pre-existing aqueous pathways associated with sweat gland ducts and hair follicles. Many experimental studies¹ have probed the action of penetration enhancers, and three major enhancement mechanisms have been suggested: (1) interactions with intercellular lipids of the SC, which leads to a disorganization of these highly ordered structures and, thus, enhances the paracellular diffusivity through the SC; (2) interactions with intracellular proteins of the corneocytes to increase transcellular permeation; and (3) increasing the partitioning of the drug into the SC.

METHODS

1. Selection of Training Sets. MI-QSAR analysis focuses upon the uptake and transport of organic compounds in a phospholipid monolayer or bilayer assembly, which are normally used as models for cellular membranes, and/or lipid-rich media. In other words, MI-QSAR analysis focuses upon the behavior of organic compounds in a nonpolar, lipidlike medium like the SC. Thus, the MI-QSAR skin penetration enhancer studies carried out in this work have been limited to nonpolar skin penetration enhancers, but both hydrocortisone (HC) and hydrocortisone acetate (HCA) as reference penetrants have been considered. Specifically, two of the skin penetration enhancer data sets used in our previous study¹ were also employed in this study. These data sets are as follows.

Training Set 1. The training set consists of 61 surfactant-like and nonpolar enhancers for which penetration enhancement was measured using HC as a master reference penetrator.^{5,7–14} The measure of skin penetration enhancement, denoted by $ER(J)$, is the ratio of the HC penetration with, and without, a common fixed concentration of the test enhancer. The first $ER(J)$ entry for these enhancers in Table 1 was used to build the QSAR models. The first listed measurements of $ER(J)$ reported in Table 1 represent self-consistent data because they come from the same laboratory or, at the very least, from one common experimental protocol so as to minimize measured end-point variations in the data. $\log ER(J)$ was the actual representation for penetration enhancement used in constructing the QSAR models of our original study, but $ER(J)$ could be used directly in the MI-QSAR analyses reported in this paper.

The in vitro skin penetration enhancement measurement method has been described in refs 7–16 and is only summarized here. The skin permeation parameters were determined by plotting the cumulative drug amount permeated through the skin versus time. The slope of the linear portion of the permeation curve provided the flux value (J ; $\text{mg cm}^{-2} \text{ h}^{-1}$) at a steady state. The $ER(J)$ for flux was calculated as

$$ER(J) = \frac{[\text{flux for skin treated with enhancer}]}{[\text{flux for control}]} \quad (1)$$

for which the flux for control denotes when the skin is untreated with the enhancer.

Training Set 2. This training set consists mainly of surfactant-like and nonpolar enhancers for which penetration enhancement was measured using HCA as a master reference

penetrator.^{9,13–16} The measure of penetration enhancement is the same as for training set 1.

Again, the first $ER(J)$ entry for each enhancer was used to build the QSAR models for the same reason as explained for Table 1. There are 42 skin penetration enhancers in this training set, which are given in Table 2.

2. The MI-QSAR Paradigm. *A. Modeling of the Penetration Enhancer Molecules and the DMPC Phospholipid Monolayer.* The MI-QSAR paradigm has been discussed in detail previously and is only summarized here.^{2,3,17–19} Currently, this methodology uses a model membrane monolayer, or bilayer, composed of packed dimyristoylphosphatidylcholine (DMPC) molecules. Only monolayers have been considered in this work. The DMPC molecule is modeled from available crystal structure data.²⁰ The structure of a DMPC molecule is shown in Figure 1. An assembly of 25 DMPC molecules ($5 \times 5 \times 1$) in x , y , and z directions, respectively, forms the model membrane monolayer (Figure 2). Additional information regarding the construction of the monolayer model can be found in refs 2, 3, and 17–19.

The DMPC molecule and the penetration enhancers of both training sets were built using the HyperChem program.²¹ The AM1 Hamiltonian in Mopac 6.0²² was used to estimate the partial atomic charge distribution over each molecule.

B. Molecular Dynamic Simulations. The conditions used in the MDS were established in previous MI-QSAR analyses^{2,3,17–19} and are only summarized here. An initial MDS was carried out on the model membrane, without a solute molecule present, to allow structural relaxation and the distribution of the kinetic energy over the monolayer. In order to prevent unfavorable van der Waals interactions between a penetration enhancer and the DMPC molecules of the membrane, one of the “center” DMPC molecules was removed from the equilibrated monolayer. The penetration enhancer under consideration was then inserted into the space vacated by the DMPC molecule that was removed. Typically, each of the penetration enhancers of the two data sets in Tables 1 and 2 was inserted at three different positions (depths) into the DMPC monolayer with the most polar group of the enhancer “facing” toward the headgroup region of the monolayer. Three corresponding MDS trajectory sets were generated for each skin penetration enhancer with regard to the trial positions it was assigned in the monolayer. The three trial positions are (1) the penetration enhancer in the headgroup region, (2) the penetration enhancer in between the headgroup region and the aliphatic chains, and (3) the penetration enhancer in the tail region of the aliphatic chains.

The lowest-energy geometry of the penetration enhancer in the monolayer was sought using each of the three trial solute positions. These lowest-energy geometries of the penetration-enhancer–monolayer complex are normally used as the starting points in each of three respective MDSs. However, virtually all of the skin penetration enhancers in training sets 1 and 2 are similar in size and shape to DMPC. Therefore, it was only necessary to explore the penetration enhancer–DMPC monolayer assembly corresponding to the first trial solute position described above. Only a single penetration enhancer molecule was explicitly considered in each MDS, and this embedded molecule was aligned within the DMPC monolayer assembly such that the most polar portion of the penetration enhancer was “facing” toward the

Table 1. Training Set 1, Consisting of 61 Nonpolar Enhancers Using Hydrocortisone (HC) as a Master Reference Penetrator

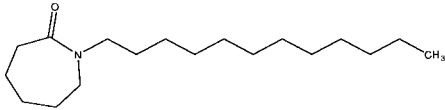
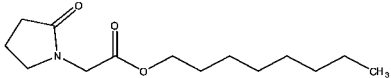
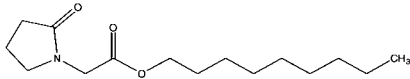
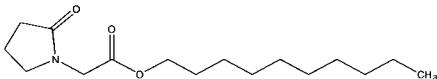
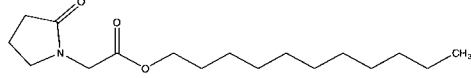
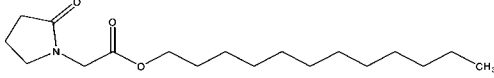
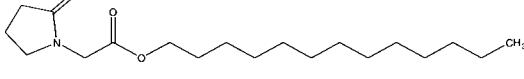
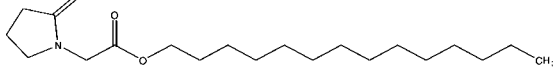
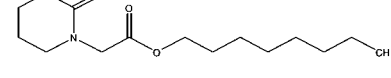
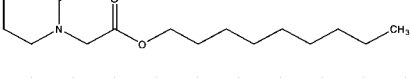
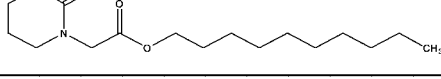
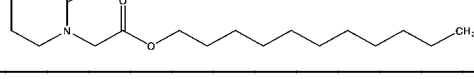
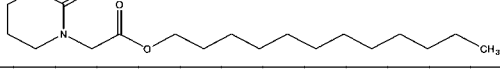
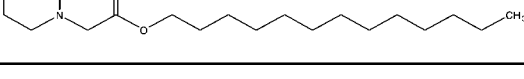
Code	Structure	ER(J)	Reference
REF-AZONE/HC-1		(a) 19.51 (b) 42.20 (c) 18.00	(a) Michniak et. al. <i>Int. J. Pharm.</i> 1995 , 116, 201-209; (b) Michniak et. al. <i>Int. J. Pharm.</i> 1998 , 161, 169-178; (c) Fuhrman Jr. et. al. <i>J. Controlled Release</i> 1997 , 45, 199-206.
SL-LACTAM-ACETIC-ESTERS/HC-1		18.89	Michniak et. al. <i>J. Pharm. Sci.</i> 1996 , 85 (2), 150-154
SL-LACTAM-ACETIC-ESTERS/HC-2		17.55	Michniak et. al. <i>J. Pharm. Sci.</i> 1996 , 85 (2), 150-154
SL-LACTAM-ACETIC-ESTERS/HC-3		38.22	Michniak et. al. <i>J. Pharm. Sci.</i> 1996 , 85 (2), 150-154
SL-LACTAM-ACETIC-ESTERS/HC-4		15.33	Michniak et. al. <i>J. Pharm. Sci.</i> 1996 , 85 (2), 150-154
SL-LACTAM-ACETIC-ESTERS/HC-5		67.33	Michniak et. al. <i>J. Pharm. Sci.</i> 1996 , 85 (2), 150-154
SL-LACTAM-ACETIC-ESTERS/HC-6		18.00	Michniak et. al. <i>J. Pharm. Sci.</i> 1996 , 85 (2), 150-154
SL-LACTAM-ACETIC-ESTERS/HC-7		25.78	Michniak et. al. <i>J. Pharm. Sci.</i> 1996 , 85 (2), 150-154
SL-LACTAM-ACETIC-ESTERS/HC-8		18.44	Michniak et. al. <i>J. Pharm. Sci.</i> 1996 , 85 (2), 150-154
SL-LACTAM-ACETIC-ESTERS/HC-9		13.33	Michniak et. al. <i>J. Pharm. Sci.</i> 1996 , 85 (2), 150-154
SL-LACTAM-ACETIC-ESTERS/HC-10		12.67	Michniak et. al. <i>J. Pharm. Sci.</i> 1996 , 85 (2), 150-154
SL-LACTAM-ACETIC-ESTERS/HC-11		36.44	Michniak et. al. <i>J. Pharm. Sci.</i> 1996 , 85 (2), 150-154
SL-LACTAM-ACETIC-ESTERS/HC-12		23.78	Michniak et. al. <i>J. Pharm. Sci.</i> 1996 , 85 (2), 150-154
SL-LACTAM-ACETIC-ESTERS/HC-13		12.00	Michniak et. al. <i>J. Pharm. Sci.</i> 1996 , 85 (2), 150-154

Table 1. Continued

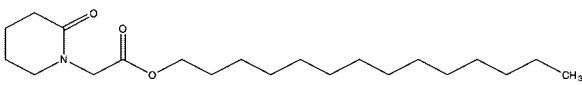
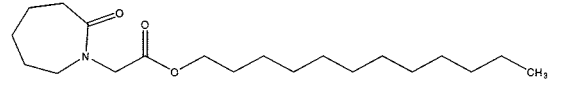
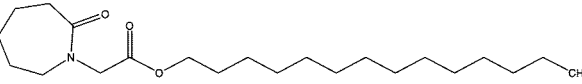
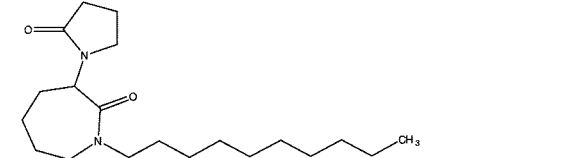
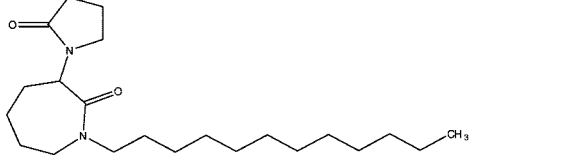
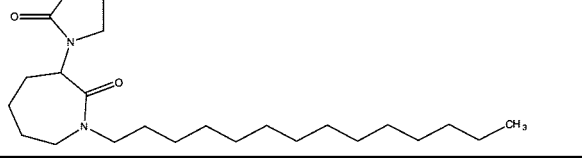
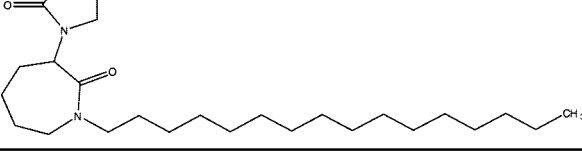
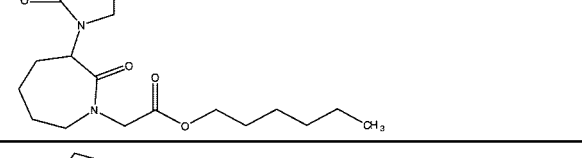
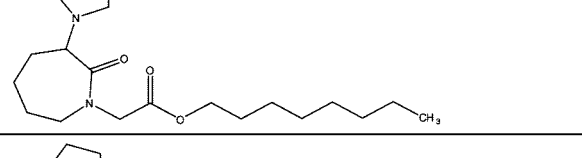
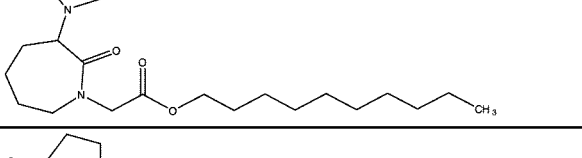
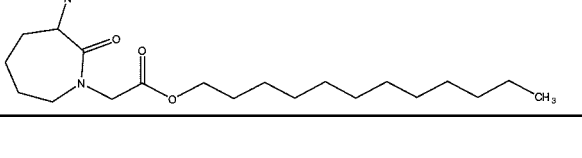
Code	Structure	ER(J)	Reference
SL-LACTAM-ACETIC-ESTERS/HC-14		37.77	Michniak et. al. <i>J. Pharm. Sci.</i> 1996 , 85 (2), 150-154
SL-LACTAM-ACETIC-ESTERS/HC-15		1.13	Michniak et. al. <i>J. Pharm. Sci.</i> 1996 , 85 (2), 150-154
SL-LACTAM-ACETIC-ESTERS/HC-16		1.96	Michniak et. al. <i>J. Pharm. Sci.</i> 1996 , 85 (2), 150-154
SL-PYRROLIDINE/HC-3		25.70	Kim et. al. <i>J. Controlled Release</i> 2001 , 73, 183-196
SL-PYRROLIDINE/HC-4		27.50	Kim et. al. <i>J. Controlled Release</i> 2001 , 73, 183-196
SL-PYRROLIDINE/HC-5		40.50	Kim et. al. <i>J. Controlled Release</i> 2001 , 73, 183-196
SL-PYRROLIDINE/HC-6		12.80	Kim et. al. <i>J. Controlled Release</i> 2001 , 73, 183-196
AM-PYRROLIDINE/HC-8		2.30	Kim et. al. <i>J. Controlled Release</i> 2001 , 73, 183-196
SL-PYRROLIDINE/HC-9		5.90	Kim et. al. <i>J. Controlled Release</i> 2001 , 73, 183-196
SL-PYRROLIDINE/HC-10		10.90	Kim et. al. <i>J. Controlled Release</i> 2001 , 73, 183-196
SL-PYRROLIDINE/HC-11		15.00	Kim et. al. <i>J. Controlled Release</i> 2001 , 73, 183-196

Table 1. Continued

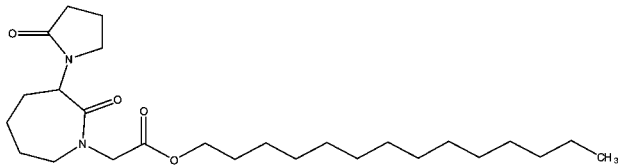
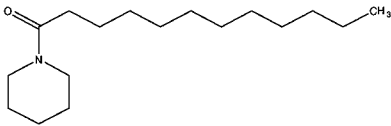
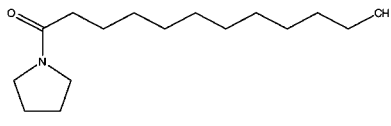
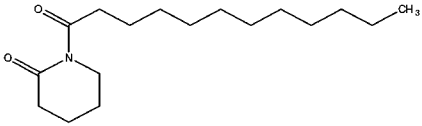
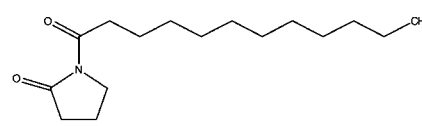
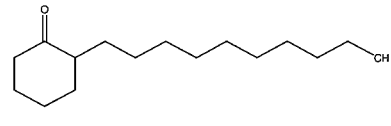
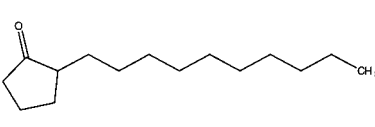
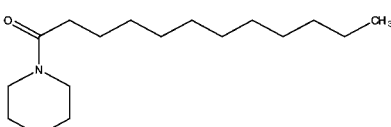
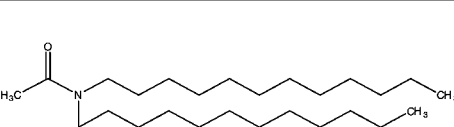
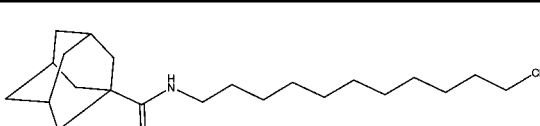
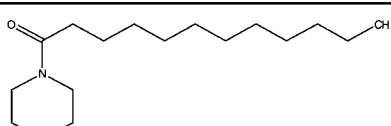
Code	Structure	ER(J)	Reference
SL-PYRROLIDINE/HC-12		16.10	Kim et. al. <i>J. Controlled Release</i> 2001 , <i>73</i> , 183-196
SL-AMIDE/HC-1		18.90	Michniak et. al. <i>Int. J. Pharm.</i> 1998 , <i>161</i> , 169-178
SL-AMIDE/HC-2		45.50	Michniak et. al. <i>Int. J. Pharm.</i> 1998 , <i>161</i> , 169-178
SL-AMIDE/HC-3		8.60	Michniak et. al. <i>Int. J. Pharm.</i> 1998 , <i>161</i> , 169-178
SL-AMIDE/HC-4		12.80	Michniak et. al. <i>Int. J. Pharm.</i> 1998 , <i>161</i> , 169-178
SL-AMIDE/HC-5		10.30	Michniak et. al. <i>Int. J. Pharm.</i> 1998 , <i>161</i> , 169-178
SL-AMIDE/HC-6		8.20	Michniak et. al. <i>Int. J. Pharm.</i> 1998 , <i>161</i> , 169-178
SL-AMIDE/HC-7		32.90	Michniak et. al. <i>Int. J. Pharm.</i> 1998 , <i>161</i> , 169-178
SL-AMIDE/HC-8		9.20	Michniak et. al. <i>Int. J. Pharm.</i> 1998 , <i>161</i> , 169-178
SL-AMIDE/HC-11		5.00	Michniak et. al. <i>Int. J. Pharm.</i> 1998 , <i>161</i> , 169-178
SL-AMIDE/HC-12		(a) 56.40 (b) 26.22	(a) Michniak et. al. <i>Int. J. Pharm.</i> 1998 , <i>161</i> , 169-178; (b) Michniak et. al. <i>Int. J. Pharm.</i> 1993 , <i>94</i> , 203-210

Table 1. Continued

Code	Structure	ER(J)	Reference
SL-AMIDE/HC-13		(a) 60.10 (b) 21.30 (c) 38.04	(a) Michniak et. al. <i>Int. J. Pharm.</i> 1998 , 161, 169-178; (b) Fuhrman Jr. et. al. <i>J. Controlled Release</i> 1997 , 45, 199-206; (c) Michniak et. al. <i>Int. J. Pharm.</i> 1993 , 94, 203-210
SL-AMIDE/HC-14		(a) 48.30 (b) 20.60 (c) 53.80	(a) Michniak et. al. <i>Int. J. Pharm.</i> 1998 , 161, 169-178; (b) Fuhrman Jr. et. al. <i>J. Controlled Release</i> 1997 , 45, 199-206; (c) Michniak et. al. <i>Int. J. Pharm.</i> 1993 , 94, 203-210
SM-DIOXOLANES/HC-1		0.93	Michniak et. al. <i>Drug Deliv.</i> 1995 , 2, 117-122
SL-DIOXOLANES/HC-2		(a) 6.13 (b) 6.10	(a) Michniak et. al. <i>Drug Deliv.</i> 1995 , 2, 117-122; (b) Fuhrman Jr. et. al. <i>J. Controlled Release</i> 1997 , 45, 199-206
SL-DIOXOLANES/HC-3		2.63	Michniak et. al. <i>Drug Deliv.</i> 1995 , 2, 117-122
SM-DIOXOLANES/HC-4		0.70	Michniak et. al. <i>Drug Deliv.</i> 1995 , 2, 117-122
SL-DIOXOLANES/HC-5		2.17	Michniak et. al. <i>Drug Deliv.</i> 1995 , 2, 117-122
SL-DIOXOLANES/HC-6		1.57	Michniak et. al. <i>Drug Deliv.</i> 1995 , 2, 117-122
SM-DIOXOLANES/HC-7		1.03	Michniak et. al. <i>Drug Deliv.</i> 1995 , 2, 117-122
SL-DIOXOLANES/HC-8		2.40	Michniak et. al. <i>Drug Deliv.</i> 1995 , 2, 117-122
SL-DIOXOLANES/HC-9		2.50	Michniak et. al. <i>Drug Deliv.</i> 1995 , 2, 117-122
SM-DIOXOLANES/HC-10		0.63	Michniak et. al. <i>Drug Deliv.</i> 1995 , 2, 117-122
SL-DIOXOLANES/HC-11		1.40	Michniak et. al. <i>Drug Deliv.</i> 1995 , 2, 117-122

Table 2. Training Set 2, Consisting of 42 Nonpolar Enhancers Using Hydrocortisone Acetate (HCA) as a Master Reference Penetrator

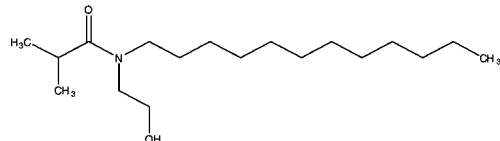
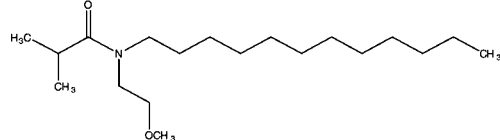
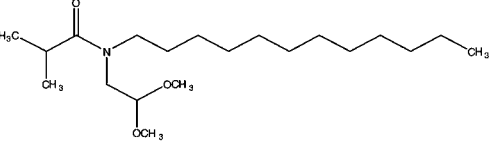
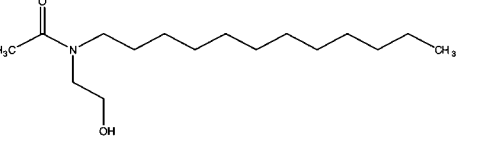
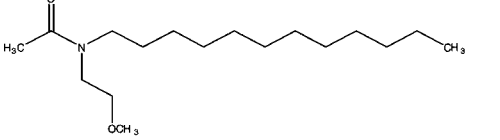
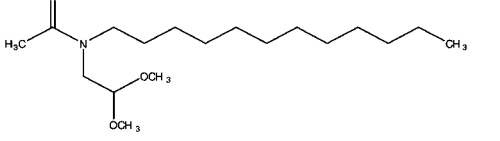
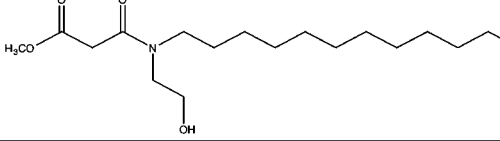
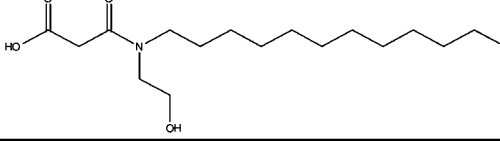
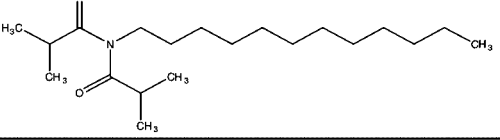
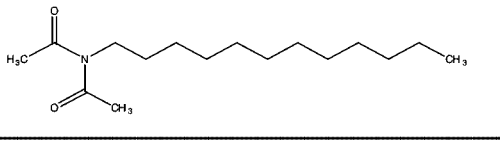
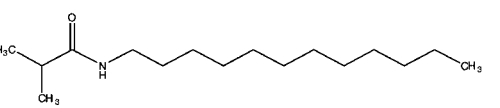
Code	Structure	ER(J)	Reference
SL-ACYCLIC-AZONE-AMIDES/HCA-1		13.62	Michniak et. al. <i>Int. J. Pharm.</i> 1994 , <i>110</i> , 231-239
SL-ACYCLIC-AZONE-AMIDES/HCA-2		(a) 20.80 (b) 5.00	(a) Michniak et. al. <i>Int. J. Pharm.</i> 1994 , <i>110</i> , 231-239; (b) Fuhrman Jr. et. al. <i>J. Controlled Release</i> 1997 , <i>45</i> , 199-206.
SL-ACYCLIC-AZONE-AMIDES/HCA-3		20.02	Michniak et. al. <i>Int. J. Pharm.</i> 1994 , <i>110</i> , 231-239
SL-ACYCLIC-AZONE-AMIDES/HCA-4		25.78	Michniak et. al. <i>Int. J. Pharm.</i> 1994 , <i>110</i> , 231-239
SL-ACYCLIC-AZONE-AMIDES/HCA-5		(a) 35.22 (b) 13.00	(a) Michniak et. al. <i>Int. J. Pharm.</i> 1994 , <i>110</i> , 231-239; (b) Fuhrman Jr. et. al. <i>J. Controlled Release</i> 1997 , <i>45</i> , 199-206.
SL-ACYCLIC-AZONE-AMIDES/HCA-6		24.53	Michniak et. al. <i>Int. J. Pharm.</i> 1994 , <i>110</i> , 231-239
SL-ACYCLIC-AZONE-AMIDES/HCA-7		14.22	Michniak et. al. <i>Int. J. Pharm.</i> 1994 , <i>110</i> , 231-239
SL-ACYCLIC-AZONE-AMIDES/HCA-8		5.67	Michniak et. al. <i>Int. J. Pharm.</i> 1994 , <i>110</i> , 231-239
SL-ACYCLIC-AZONE-AMIDES/HCA-9		5.87	Michniak et. al. <i>Int. J. Pharm.</i> 1994 , <i>110</i> , 231-239
SL-ACYCLIC-AZONE-AMIDES/HCA-10		14.24	Michniak et. al. <i>Int. J. Pharm.</i> 1994 , <i>110</i> , 231-239
SL-ACYCLIC-AZONE-AMIDES/HCA-11		57.38	Michniak et. al. <i>Int. J. Pharm.</i> 1994 , <i>110</i> , 231-239

Table 2. Continued

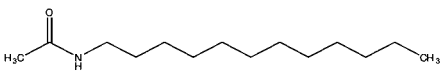
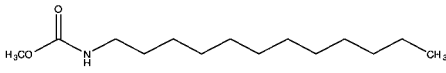
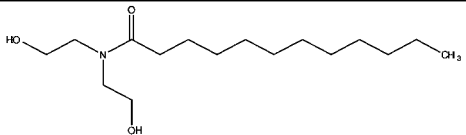
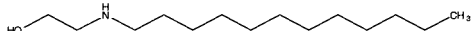
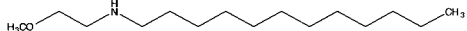
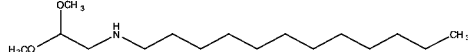
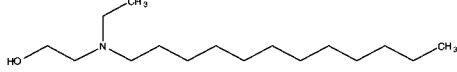
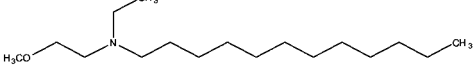
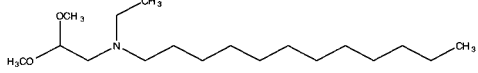
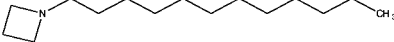
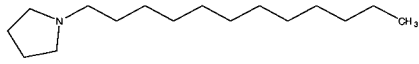
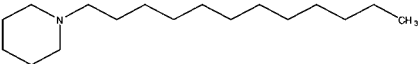
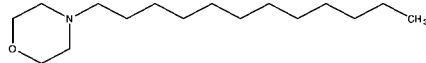
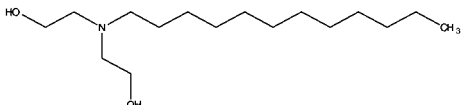
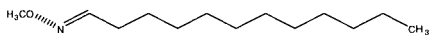
Code	Structure	ER(J)	Reference
SL-ACYCLIC-AZONE-AMIDES/HCA-12		29.38	Michniak et. al. <i>Int. J. Pharm.</i> 1994 , 110, 231-239
SL-ACYCLIC-AZONE-AMIDES/HCA-13		6.51	Michniak et. al. <i>Int. J. Pharm.</i> 1994 , 110, 231-239
SL-ACYCLIC-AZONE-AMIDES/HCA-14		10.02	Michniak et. al. <i>Int. J. Pharm.</i> 1994 , 110, 231-239
SL-AZONE-AMINES/HCA-1		11.80	Michniak et. al. <i>Int. J. Pharm.</i> 1995 , 116, 201-209;
SL-AZONE-AMINES/HCA-2		16.00	Michniak et. al. <i>Int. J. Pharm.</i> 1995 , 116, 201-209;
SL-AZONE-AMINES/HCA-3		13.18	Michniak et. al. <i>Int. J. Pharm.</i> 1995 , 116, 201-209;
SL-AZONE-AMINES/HCA-4		9.16	Michniak et. al. <i>Int. J. Pharm.</i> 1995 , 116, 201-209;
SL-AZONE-AMINES/HCA-5		30.89	Michniak et. al. <i>Int. J. Pharm.</i> 1995 , 116, 201-209;
SL-AZONE-AMINES/HCA-6		8.04	Michniak et. al. <i>Int. J. Pharm.</i> 1995 , 116, 201-209;
SL-AZONE-AMINES/HCA-7		17.80	Michniak et. al. <i>Int. J. Pharm.</i> 1995 , 116, 201-209;
SL-AZONE-AMINES/HCA-8		9.87	Michniak et. al. <i>Int. J. Pharm.</i> 1995 , 116, 201-209;
SL-AZONE-AMINES/HCA-9		15.33	Michniak et. al. <i>Int. J. Pharm.</i> 1995 , 116, 201-209;
SL-AZONE-AMINES/HCA-10		25.56	Michniak et. al. <i>Int. J. Pharm.</i> 1995 , 116, 201-209;
SL-AZONE-AMINES/HCA-11		(a) 16.11 (b) 7.00	(a) Michniak et. al. <i>Int. J. Pharm.</i> 1995 , 116, 201-209; (b) Fuhrman Jr. et. al. <i>J. Controlled Release</i> 1997 , 45, 199-206.
SL-AZONE-AMINES/HCA-12		13.84	Michniak et. al. <i>Int. J. Pharm.</i> 1995 , 116, 201-209;

Table 2. Continued

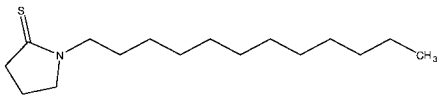
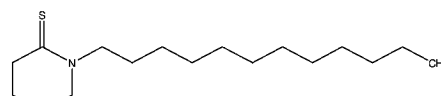
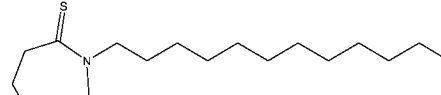
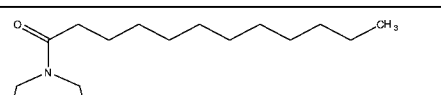
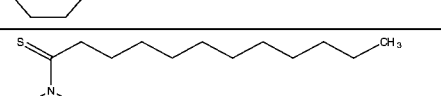
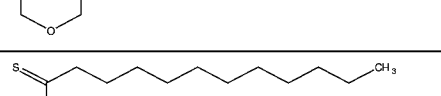
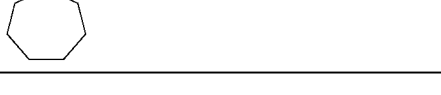
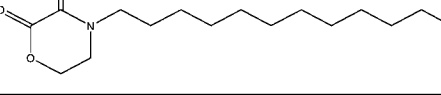
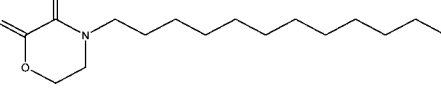
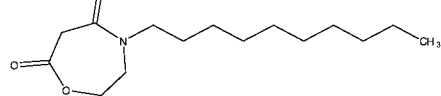
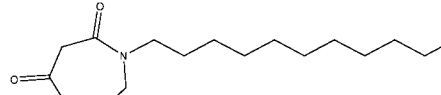
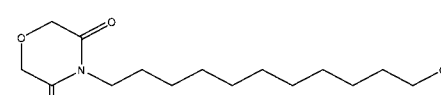
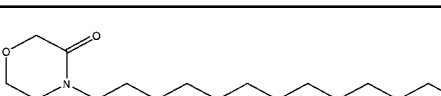
Code	Structure	ER(J)	Reference
SL-AZONE-THIO-AMIDE/HCA-3		13.71	Michniak et. al. <i>Int. J. Pharm.</i> 1993 , 94, 203-210
SL-AZONE-THIO-AMIDE/HCA-4		8.56	Michniak et. al. <i>Int. J. Pharm.</i> 1993 , 94, 203-210
SL-AZONE-THIO-AMIDE/HCA-5		4.33	Michniak et. al. <i>Int. J. Pharm.</i> 1993 , 94, 203-210
SL-AZONE-THIO-AMIDE/HCA-7		34.02	Michniak et. al. <i>Int. J. Pharm.</i> 1993 , 94, 203-210
SL-AZONE-THIO-AMIDE/HCA-8		2.09	Michniak et. al. <i>Int. J. Pharm.</i> 1993 , 94, 203-210
SL-AZONE-THIO-AMIDE/HCA-9		7.56	Michniak et. al. <i>Int. J. Pharm.</i> 1993 , 94, 203-210
SL-AZONE/HCA-3		7.09	Michniak et. al. <i>Int. J. Pharm.</i> 1993 , 91, 85-93
SL-AZONE/HCA-4		5.20	Michniak et. al. <i>Int. J. Pharm.</i> 1993 , 91, 85-93
SL-AZONE/HCA-5		44.96	Michniak et. al. <i>Int. J. Pharm.</i> 1993 , 91, 85-93
SL-AZONE/HCA-6		12.67	Michniak et. al. <i>Int. J. Pharm.</i> 1993 , 91, 85-93
SL-AZONE/HCA-7		10.20	Michniak et. al. <i>Int. J. Pharm.</i> 1993 , 91, 85-93
SL-AZONE/HCA-8		14.07	Michniak et. al. <i>Int. J. Pharm.</i> 1993 , 91, 85-93
SL-AZONE/HCA-9		18.80	Michniak et. al. <i>Int. J. Pharm.</i> 1993 , 91, 85-93

Table 2. Continued

Code	Structure	ER(J)	Reference
SL-AZONE/HCA-10		12.24	Michniak et. al. <i>Int. J. Pharm.</i> 1993 , 91, 85-93
SL-AZONE/HCA-11		14.38	Michniak et. al. <i>Int. J. Pharm.</i> 1993 , 91, 85-93
SL-AZONE/HCA-12		20.00	Michniak et. al. <i>Int. J. Pharm.</i> 1993 , 91, 85-93

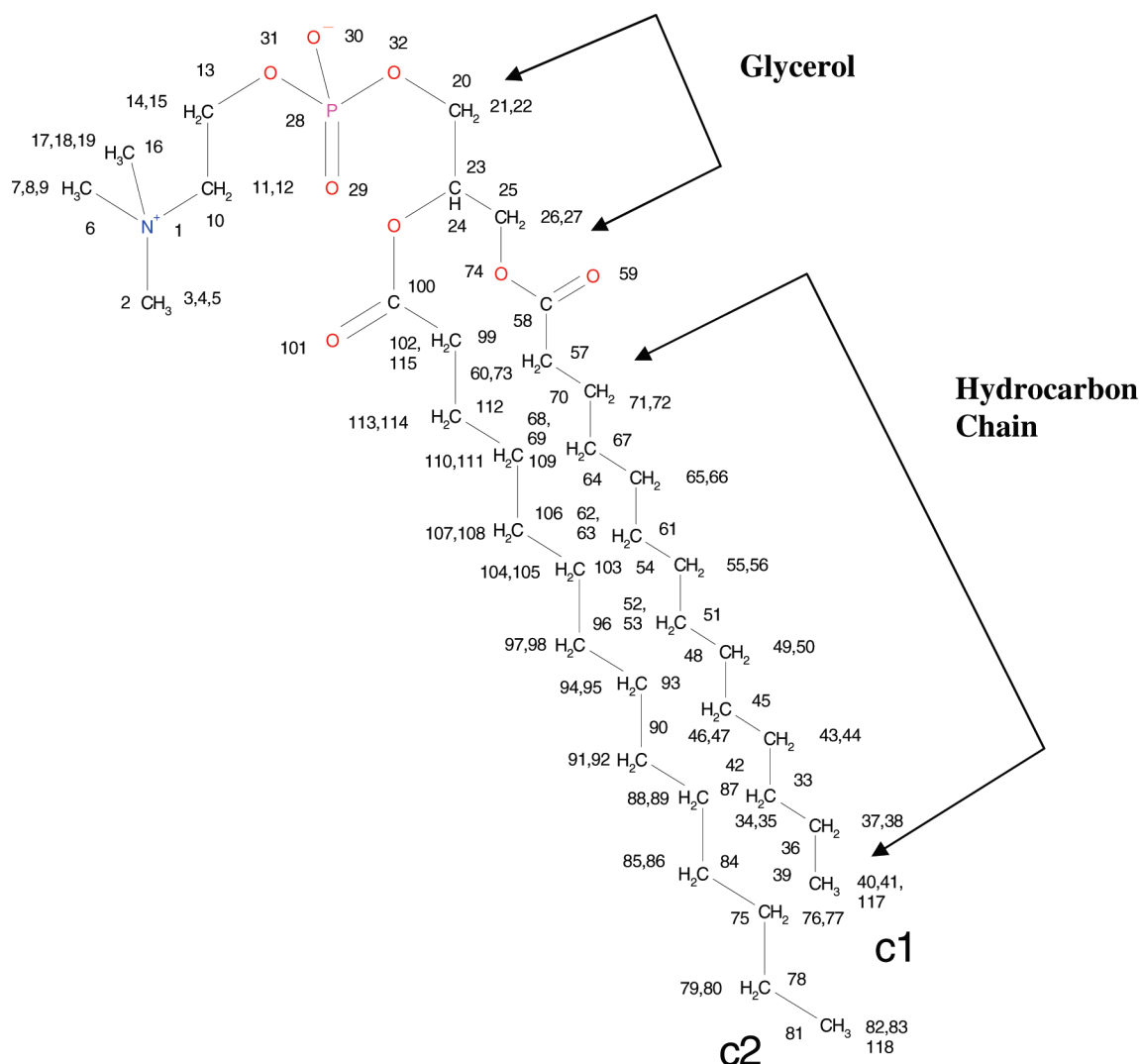


Figure 1. The chemical structure of a DMPC phospholipid molecule with an arbitrary atom numbering assignment. **C1** and **C2** denote the two aliphatic chains of a DMPC molecule.

3, but those most often used in traditional QSAR studies are listed and have been used in this work. Table 3 is divided into intramolecular and intermolecular descriptor sets as a reminder that, although all of these descriptors are computed from a methodology based solely on the structure of an

individual molecule, some of these descriptors are actually measures of intermolecular interactions. $F(\text{H}_2\text{O})$, $F(\text{oct})$, and LogP , the aqueous and 1-octanol solvation free energies and the corresponding 1-octanol/water partition coefficient of the penetration enhancer, respectively, are intermolecular proper-

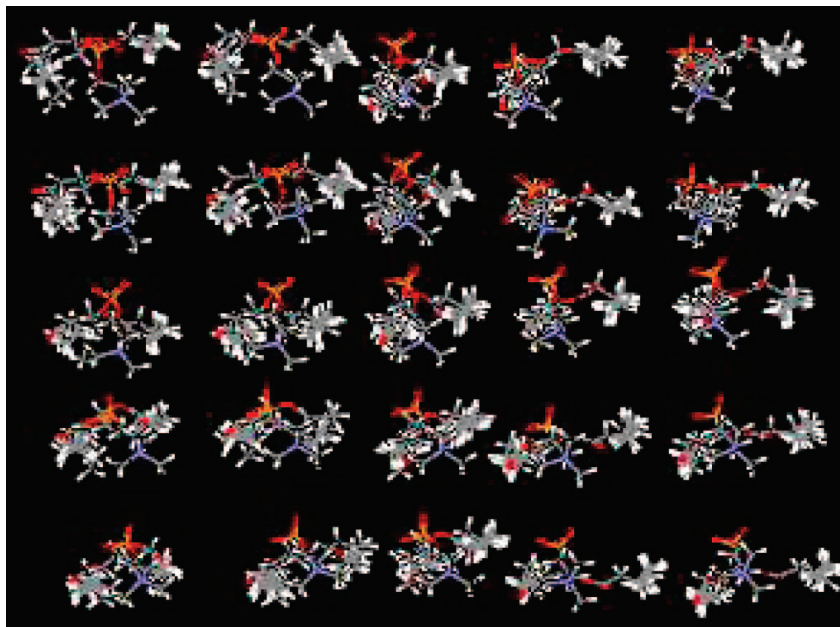


Figure 2. Top view of the DMPC monolayer assembly before MDS relaxation.

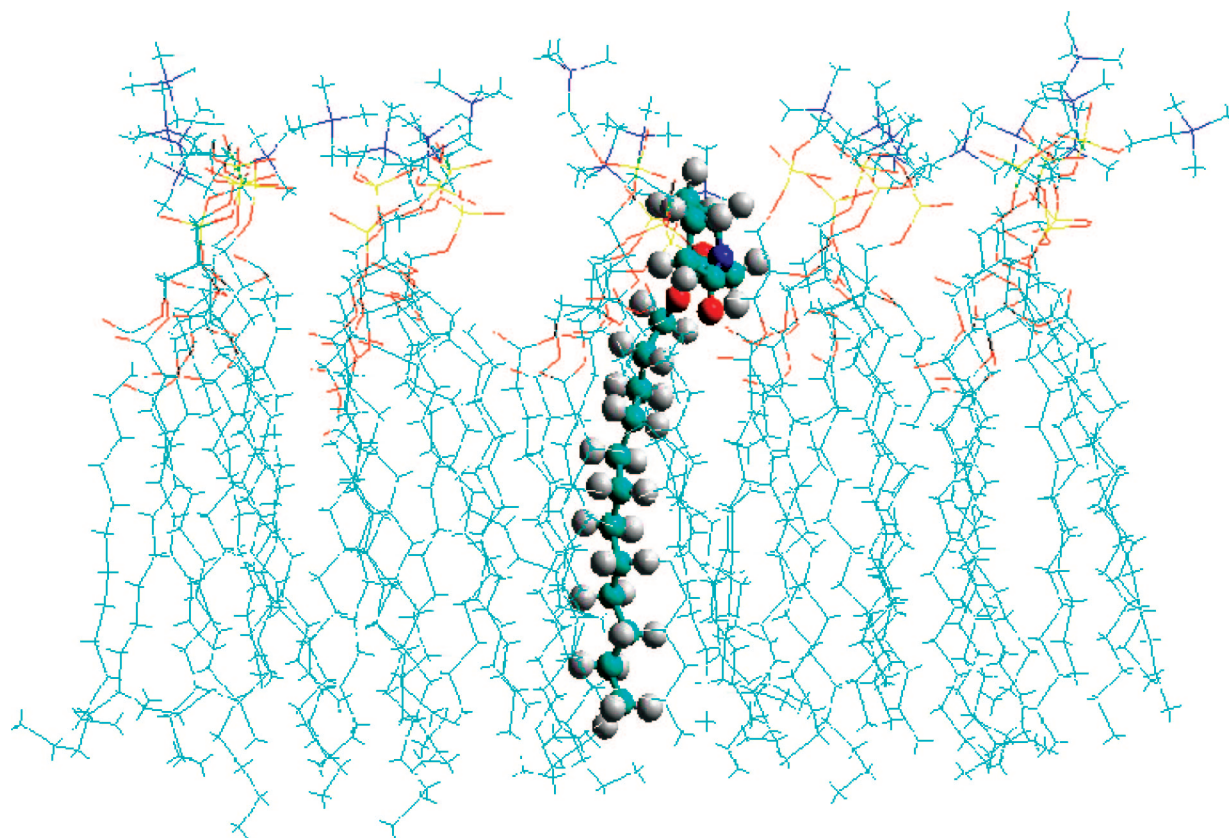


Figure 3. The energetically most favorable geometry of a potent penetration enhancer, HC-5 of Table 1, in the DMPC monolayer, taken from its MDS trajectory.

ties relating to solute solvation. $E(\text{coh})$, T_M , and T_G , are the cohesive energy and the hypothetical crystal-melt and glass transition temperatures of the penetration enhancers, respectively, which are used to estimate solute dissolution behavior.

The *intermolecular solute–membrane interaction descriptors* are extracted directly from the MDS trajectories and are listed in Table 4. These particular intermolecular descriptors are calculated using the most stable (lowest total potential energy) penetration enhancer–membrane geometry realized

from the MDS sampling of each penetration enhancer. But we have now come to recognize the need in MI-QSAR models for descriptors which capture the time-average change in the structure of the monolayer molecular assembly due to the presence of an embedded molecule, in this case, a penetration enhancer. A descriptor which meets this need is the integrated difference in the monolayer cylindrical distribution function, CDF, for the monolayer in and out of the presence of the embedded molecule.

Table 3. The Classic Set of QSAR Descriptors

Intramolecular	
HOMO	highest occupied molecular orbital energy
LUMO	lowest unoccupied molecular orbital energy
Dp	dipole moment
Vm	molecular volume
SA	molecular surface area
Ds	density
MW	molecular weight
MR	molecular refractivity
N(hba)	number of hydrogen bond acceptors
N(hbd)	number of hydrogen bond donors
N(B)	number of rotatable bonds
JSSA (X)	Jurs–Stanton surface area descriptors
Chi-N, Kappa-M	Kier and Hall topological descriptors
Rg	radius of gyration
PM	principle moment of inertia
PSA	polar surface area
Se	conformational entropy
Q(I)	partial atomic charge densities
Intermolecular	
F(H ₂ O)	aqueous solva aqueous solvation free energy
F(oct)	1-octanol solvation free energy
LogP	1-octanol/water partition coefficient
Ecoh	cohesive packing energy
T _M	hypothetical crystal-melt transition temperature
T _G	hypothetical glass transition temperature

The radial distribution function (RDF)²⁵ is an example of a pair correlation function which describes how, on average, the “particles” in a multiparticle system are spherically packed around one another. This proves to be a particularly effective way of describing the average structure of semi- and disordered molecular systems such as liquids. Also, in molecular systems like liquids, there is continual movement of the constituent atoms, and a single snapshot of the system provides only a single instantaneous structural representation of the system. In such cases, it is extremely useful to be able to deal with representations of the average structure of the system over time, which the RDF makes possible. Usually, when using MDS, the RDF is calculated by using following equation:

$$g(r) = n(r) / (\rho * 4\pi r^2 * dr) \quad (2)$$

in which $g(r)$ is the RDF, $n(r)$ is the mean number of particles (atoms) in a shell of width dr at distance r from an arbitrary particle or position, and ρ is the mean particle density. In a previous study,²⁶ the RDF for a pure DMPC monolayer assembly and the RDF of a mixed DMPC–DMTAP (dimyristoyltrimethyl-ammonium propane) monolayer assembly were determined and compared. The location and shapes of the main peaks of these two RDFs are much different from one another, reflecting the different average molecular packing behavior of these two monolayer assemblies. But the RDFs also demonstrate the sensitivity of a time-averaged distribution function to the structure and dynamics of the phospholipid assemblies being sampled.

Still, the DMPC molecules forming the monolayer have long “cylindrical” axes and pack together with respect to these long cylindrical axes. Thus, this type of molecular assembly is characterized by cylindrical symmetry, and hence, a corresponding CDF is defined and employed to estimate and represent the average structure of the system over time. The DMPC CDF used in this study is defined as

$$h(r) = n(r) / (\rho * 2\pi r * dr) \quad (3)$$

where $h(r)$ is the CDF, $n(r)$ is the mean number of atoms in a cylindrical-shaped shell of width dr (0.2 Å in this study) at distance r from an arbitrary helical axis, and ρ is the mean

DMPC monolayer density. A schematic top view of the monolayer assembly with the cylindrical shell used to compute $n(r)$ is shown in Figure 4. The CDF in this particular application offers the opportunity to obtain a finer spatial resolution than can be had from the RDF by taking advantage of the inherent cylindrical symmetry of the molecular assemblies being studied.

The CDF by itself simply portrays the time-average spatial distribution of the DMPC molecules of the monolayer with, or without, in this case, a skin penetration enhancer embedded within the monolayer. While both are useful and insightful, this representation of the behavior of the monolayer cannot be used in a QSAR analysis. What is needed is a composite *scalar* measure of the change in the average spatial structure of the monolayer due to the presence of an embedded molecule (skin penetration enhancer in this case) as compared to when the embedded molecule is absent. The integrated spatial difference, $\Delta \sum h(r)$, between the embedded molecule, present CDF, and the CDF of the embedded molecule, absent, is such a scalar measure and a corresponding MI-QSAR descriptor:

$$\Delta \sum h(r) = \int_{r_i}^{r_f} |h_S(r) - h_M(r)| dr \quad (4)$$

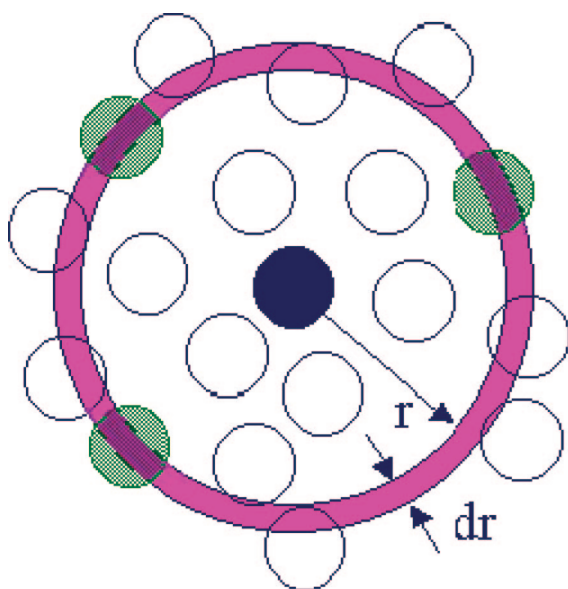
In eq 4, $h_S(r)$ is the CDF with the embedded molecule and $h_M(r)$ the CDF without any embedded molecule in the monolayer. The terms r_i and r_f are the initial and final distances, respectively, from an arbitrary center axis, normally one of the DMPC molecular axes, in which the integration of the difference in the CDFs is carried out. A combined inspection of eq 4, along with an inspection of a typical difference CDF, shown in Figure 5 for the fourth entry in Table 1, SL-LACTAM-ACETIC-ESTER/HC-3, reveals that $\Delta \sum h(r)$ is nothing more than the area within the difference CDF plot with respect to the r axis. The greater the area under the curve, relative to the r axis, the greater is the value of $\Delta \sum h(r)$ and the greater is the change in the time-averaged monolayer structure due to the embedded molecule.

To be clear, the $\Delta \sum h(r)$ values are computed using the composite MDS profile from the resultant trajectories of all three initial MDS positions of the embedded molecule (penetration enhancer) in the monolayer. In this application, however, only the initial position of the penetration enhancer in the headgroup region of the monolayer needs to be considered, owing to the similar sizes and shapes of the penetration enhancers to lipids and surfactants. The difference CDF integration is carried out from the “steric surface” of the center DMPC molecule, $r_i \approx 6$ Å, to the end of the second nearest-neighbor DMPC molecule of the monolayer, $r_f \approx 23$ Å. Perhaps the most simple interpretation of $\Delta \sum h(r)$ is that it is measuring how big of “holes” are formed in the monolayer structure due to the presence of the skin penetration enhancer.

3. Construction and Validation of the MI-QSAR Models. MI-QSAR models were built and optimized using multidimensional linear regression fitting and the genetic function approximation (GFA),^{27,28} which is a multidimensional optimization method based on the genetic algorithm paradigm. Both linear and quadratic representations of each of the descriptor values were included in the trial descriptor

Table 4. The MI-QSAR Intermolecular Solute-Membrane Descriptors

$\langle F(\text{total}) \rangle$	average total free energy of interaction of the solute and membrane
$\langle E(\text{total}) \rangle$	average total interaction energy of the solute and membrane
$E_{\text{INTER}}(\text{total})$	interaction energy between the solute and the membrane at the total intermolecular system minimum potential energy
$E_{\text{XY}}(\text{Z})_{\text{E}}$	$Z = 1,4$ -nonbonded, general van der Waals, electrostatic, hydrogen bonding, and torsion energies and combinations thereof at the total intermolecular system minimum potential energy X, Y can be the solute, S, and/or membrane, M, and if $E = \text{free}$, then $X = Y = \text{S}$ and the energies are for the solute not in the membrane, but isolated by itself
$\Delta E_{\text{XY}}(\text{Z})$	change in the $Z = 1,4$ -nonbonded, general van der Waals, electrostatic, hydrogen bonding, and torsion energies and combinations thereof due to the uptake of the solute to the total intermolecular system minimum potential energy X, Y can be the solute, S, and/or membrane, M
$E_{\text{TT}}(\text{Z})$	$Z = 1,4$ -nonbonded, general Van der Waals, electrostatic, hydrogen bonding, torsion and combinations thereof energies of the total [solute and membrane model] intermolecular minimum potential energy
$\Delta E_{\text{TT}}(\text{Z})$	change in the $Z = 1,4$ -nonbonded, general van der Waals, electrostatic, and hydrogen bonding energies and combinations thereof of the total [solute and membrane model] intermolecular minimum potential energy
ΔS	change in entropy of the membrane due to the uptake of the solute
S	absolute entropy of the solute-membrane system
$\Delta \rho$	change in density of the model membrane due to the permeating solute

**Figure 4.** A schematic top view of the monolayer geometry used to derive the CDF. The open and darkened small circles represent DMPC molecules, and the large ring represents the cylinder integration area of thickness dr at a distance r from an arbitrarily chosen DMPC cylindrical center.

pool, and MI-QSAR models were built as a function of the number of descriptor terms in a model. Statistical significance in the optimization of a QSAR model was judged jointly by the correlation coefficient of fit, R^2 , and the leave-one-out cross validation correlation coefficient, Q^2 . In addition, GFA uses Friedman's lack of fit measure to resist overfitting,

Table 5. The Results of the Random Scrambling Experiments and the Findings from the Test Set Predictions Studies for the Two Training Sets

data set ^a	$\langle R^2 \rangle^b$	$\langle Q^2 \rangle$
original training set 1: $N = 61$	0.23 – scrambled	
original training set 2: $N = 42$	0.29 – scrambled	
test training set 1: $N = 52$	0.794	0.736
test training set 2: $N = 37$	0.828	0.758
test set 1: $N = 9$	0.69	
test set 2: $N = 7$	0.71	

^a The “test training sets” are those data sets constructed from randomly extracting 15% of the compounds in the original training set and using the resultant data set to build a QSAR model. The “test sets” are the 15% of the compounds extracted from the original training set and whose activities are predicted using QSAR models built from the remaining 85% of the compounds in the original training set. N in each case is the number of compounds in the data set. ^b The $\langle R^2 \rangle$ are for the 3000 random scrambling level as described in the test.

which is a problem often encountered in constructing statistical models.²⁹

Each of the two original training sets was repeatedly subdivided, on a random selection basis, into a subtraining set and a test set. Each test set was restricted to 15% of the compounds in the original training set. A total of 70 different subtraining sets and test sets were constructed for training set 1 and 50 such sets for training set 2 to provide a sampling greater than the size of each respective original training set. MI-QSAR models were constructed in an identical fashion to those in the original training set for each corresponding

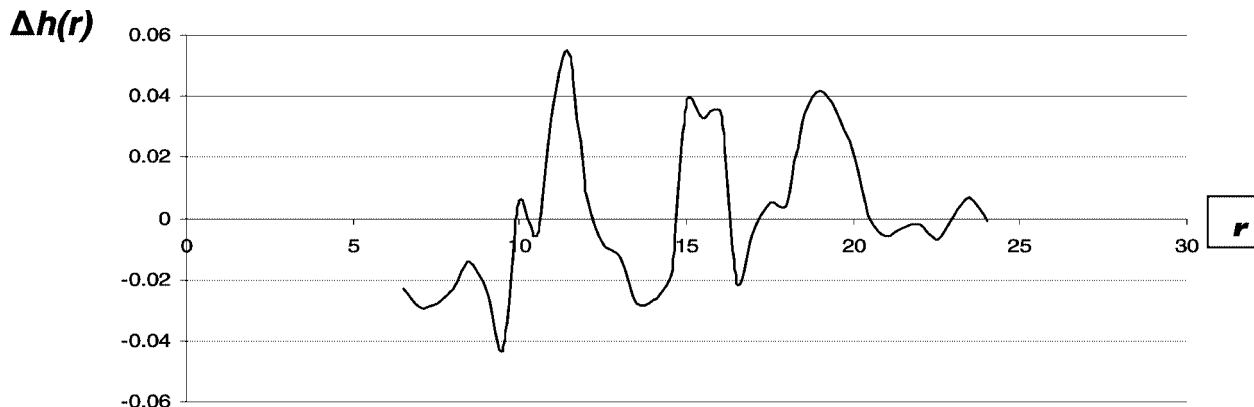
**Figure 5.** The difference CDF for the fourth entry in Table 1, SL-LACTAM-ACETIC-ESTER/HC-3.

Table 6. The ER(*J*) and Descriptor Values for the MI-QSAR Model Given by eq 5

compound code #	FH20	Dipole	ER(<i>J</i>)	$\Delta\Sigma h(r)$
REF-AZONE/HC-1	0.46	0.13	19.51	0.873
SL-LACTAM-ACETIC-ESTERS/HC-1	-2.18	0.18	18.89	1.235
SL-LACTAM-ACETIC-ESTERS/HC-2	-1.98	0.19	17.55	1.106
SL-LACTAM-ACETIC-ESTERS/HC-3	-1.78	0.19	38.22	1.744
SL-LACTAM-ACETIC-ESTERS/HC-4	-1.57	0.19	15.33	1.192
SL-LACTAM-ACETIC-ESTERS/HC-5	-1.37	0.19	67.33	1.805
SL-LACTAM-ACETIC-ESTERS/HC-6	-1.17	0.18	18.00	1.168
SL-LACTAM-ACETIC-ESTERS/HC-7	-0.96	0.18	25.78	1.255
SL-LACTAM-ACETIC-ESTERS/HC-8	-1.98	0.21	18.44	1.452
SL-LACTAM-ACETIC-ESTERS/HC-9	-1.78	0.21	13.33	1.2
SL-LACTAM-ACETIC-ESTERS/HC-10	-1.57	0.21	12.67	1.15
SL-LACTAM-ACETIC-ESTERS/HC-11	-1.37	0.21	36.44	1.527
SL-LACTAM-ACETIC-ESTERS/HC-12	-1.17	0.21	23.78	1.321
SL-LACTAM-ACETIC-ESTERS/HC-13	-0.96	0.21	12.00	1.045
SL-LACTAM-ACETIC-ESTERS/HC-14	-0.76	0.21	37.77	1.427
SL-LACTAM-ACETIC-ESTERS/HC-15	-0.96	0.2	1.13	0.455
SL-LACTAM-ACETIC-ESTERS/HC-16	-0.56	0.2	1.96	0.511
SL-PYRROLIDINE/HC-3	2.48	0.16	25.70	1.205
SL-PYRROLIDINE/HC-4	2.89	0.16	27.50	1.145
SL-PYRROLIDINE/HC-5	3.29	0.16	40.50	1.238
SL-PYRROLIDINE/HC-6	3.7	0.16	12.80	0.582
SL-PYRROLIDINE/HC-9	-2.27	0.26	5.90	0.965
SL-PYRROLIDINE/HC-10	-1.87	0.26	10.90	0.872
SL-PYRROLIDINE/HC-11	-1.46	0.26	15.00	0.922
SL-PYRROLIDINE/HC-12	-1.05	0.27	16.10	0.95
SL-AMIDE/HC-1	0.26	0.12	18.90	0.873
SL-AMIDE/HC-2	0.06	0.13	45.50	1.2
SL-AMIDE/HC-3	-0.59	0.22	8.60	0.825
SL-AMIDE/HC-4	-0.8	0.23	12.80	0.91
SL-AMIDE/HC-5	2.53	0.1	10.30	0.522
SL-AMIDE/HC-6	2.33	0.1	8.20	0.57
SL-AMIDE/HC-7	-1.6	0.1	32.90	1.163
SL-AMIDE/HC-8	3.27	0.13	9.20	0.781
SL-AMIDE/HC-11	-3.82	0.11	5.00	0.443
SL-AMIDE/HC-12	-3.9	0.1	56.40	1.351
SL-AMIDE/HC-13	0.05	0.13	60.10	1.362
SL-AMIDE/HC-14	0.26	0.13	48.30	1.348
SM-DIOXOLANES/HC-1	-5.76	0.04	0.93	0.45
SL-DIOXOLANES/HC-2	-5.35	0.04	6.13	0.83
SL-DIOXOLANES/HC-3	-4.95	0.04	2.63	0.559
SM-DIOXOLANES/HC-4	-5.41	0.04	0.70	0.37
SL-DIOXOLANES/HC-5	-5.01	0.04	2.17	0.751
SL-DIOXOLANES/HC-6	-4.6	0.04	1.57	0.71
SM-DIOXOLANES/HC-7	-5.45	0.03	1.03	0.802
SL-DIOXOLANES/HC-8	-5.04	0.03	2.40	0.596
SL-DIOXOLANES/HC-9	-4.64	0.04	2.50	0.703
SM-DIOXOLANES/HC-10	-5.1	0.04	0.63	0.488
SL-DIOXOLANES/HC-11	-4.7	0.04	1.40	0.51
SL-DIOXOLANES/HC-12	-4.29	0.04	4.17	0.662
SL-UREA/HC-2	-12.55	0.17	1.10	0.35
SL-UREA/HC-3	-8.73	0.17	1.10	0.37
SL-UREA/HC-4	-8.41	0.26	6.60	0.592
SL-UREA/HC-5	-6.5	0.18	2.40	0.781
SL-UREA/HC-6	-6.18	0.28	1.40	0.822
SL-UREA/HC-9	-10.37	0.13	1.70	0.793
SL-UREA/HC-10	-10.05	0.09	2.40	0.67
SM-ARO-SULFURANES/HC-4	-1.33	0.21	1.16	0.493
SM-ARO-SULFURANES/HC-5	-0.92	0.21	6.75	0.706
SL-DIDODECYLAMINE/HC-1	0.1	0.01	34.66	1.225
SL-DODECYLAMINE/HC-2	-5.95	0.02	16.29	1.39
SL-STEARYLAMINE/HC-3	-4.74	0.02	18.42	1.175

subtraining set. Each resulting MI-QSAR model was then used to predict the corresponding test set compounds. The average R^2 and Q^2 of the subtraining set MI-QSAR models, and the average R^2 of prediction for the test set compounds, are reported in Table 5.

Random scrambling experiments were performed to further validate the MI-QSAR models. The dependent variables,

ER(*J*), of each of the two original training sets were randomly scrambled, with respect to the trial descriptor set, in increments of 1000, beginning with 1000 random scramblings. In each instance, a MI-QSAR model was constructed to test for chance correlations. By the 3000 random scrambling level, there was no meaningful change in the average R^2 value, or its mean deviation, across the MI-QSAR models

of the random scramblings as compared to the corresponding measures from the models of the 1000 and 2000 random scrambling levels for both training sets. The average R^2 values, from the 3000 random scrambling experiments done for both training sets 1 and 2, are 0.23 and 0.29, respectively. Thus, 3000 random scramblings are considered sufficient to establish that the models generated in this study are not due to chance. These validation results, in terms of the average R^2 value across the MI-QSAR models of the random scramblings, at the 3000 random-scrambling level, are also given in Table 5.

RESULTS

An inspection of Tables 1 and 2 along with Figure 3 suggests that most of the skin penetration enhancers in both training sets have the size and general shape of a DMPC molecule. Moreover, Figure 3 also indicates they “fit into” the DMPC monolayer in much the same way as does a typical DMPC molecule. Thus, these particular skin penetration enhancers are not expected to cause individual huge disruptions in the local DMPC monolayer structure but might cause significant alterations in the average structure and dynamic behavior of the monolayer.

Moreover, since the skin penetration enhancers within and between the two training sets are rather similar, and HC and HCA are analogs to one another, it was thought that the “mechanism” of penetration enhancement might be the same for the two training sets. Thus, the two training sets were combined to see if a single “master” corresponding MI-QSAR model could be built. But no significant single MI-QSAR model could be built by combining these two training sets. Hence, this finding may be indicative of a somewhat different mechanism, or transport path, of HC versus HCA through the stratum corneum even when there is marked structural similarity among the two sets of enhancers and the two reference penetrants.

The best MI-QSAR model that could be built for training set 1 is

$$\begin{aligned} \text{ER}(J) = & -11.03 + 35.13 \times \Delta \sum h(r) + \\ & 0.93 \times \text{FH2O} - 22.76 \times \text{Dipole} \quad (5) \\ N = 61, R^2 = 0.731, Q^2 = 0.672 \end{aligned}$$

By comparison, the optimum non-MI-QSAR model¹ that could be constructed for this training set using classic QSAR descriptors is

$$\begin{aligned} \log \text{ER}(J) = & 2.04 + 0.039 \times (\text{ClogP} - 8.33)^2 - \\ & 0.0001 \times (\text{HOMO} + 242.46)^2 + 0.004 \times (\text{Kappa5} - 10)^2 - \\ & 0.008 \times (\text{FH2O} - 2.48)^2 - 0.019 \times \text{Kappa4} - 15.71)^2 - \\ & 3.259 \times \text{Dipole} \\ N = 61, R^2 = 0.732, Q^2 = 0.661 \quad (6) \end{aligned}$$

The values of $\text{ER}(J)$ and those of the descriptors used in eq 5 are given in Table 6. The definitions of the classic QSAR descriptors found in eqs 5 and 6 are given in Table 3, and $\Delta \sum h(r)$ is the integrated difference of the monolayer CDFs with, and without, each of the skin penetration enhancers present in the monolayer, as defined by eq 4.

There are several significant points to make regarding the MI-QSAR given by eq 5, both by itself and in comparison to the optimum classic QSAR model given by eq 6:

1. Only three linear descriptor terms are needed to generate the optimal MI-QSAR models for training set 1, consisting of 61 skin penetration enhancers. The quality of this model cannot be increased, in terms of both larger R^2 and larger Q^2 values, by increasing the number of descriptor terms in a model.
2. The MI-QSAR model is relatively straightforward to interpret. $\Delta \sum h(r)$ suggests that the bigger the “holes” created in the monolayer by the penetration enhancer, the greater the value of $\text{ER}(J)$. The more positive the aqueous solvation free energy (less aqueous solubility), FH2O, the greater is the skin penetration enhancement. And the smaller the average dipole moment of the skin penetration enhancer in the monolayer, the greater is $\text{ER}(J)$.
3. $\text{ER}(J)$ can be directly used to build the MI-QSAR model, eq 5, while the $\log \text{ER}(J)$ form of skin penetration enhancer potency was needed to construct the classic QSAR model, eq 6.
4. The models given by eqs 5 and 6 are virtually identical in statistical measures of quality. However, eq 5 has only three linear terms, while eq 6 has six descriptor terms, five of which are quadratic as opposed to linear.
5. Both QSAR models, eqs 5 and 6, contain FH2O and Dipole as descriptors. Therefore, it is reasonable to suggest that the descriptor terms involving ClogP, HOMO, Kappa4, and Kappa5 of the classic QSAR model are needed to capture the information residing in the MI-QSAR descriptor $\Delta \sum h(r)$ of eq 5.

The best MI-QSAR model that could be built for training set 2 is

$$\begin{aligned} \text{ER}(J) = & 14.10 - 0.286 \times \text{PSA} + 32.74 \times \\ & \Delta \sum h(r) - 1.423 \times \text{Kappa5} \quad (7) \\ N = 42, R^2 = 0.788, Q^2 = 0.711 \end{aligned}$$

The corresponding optimum non-MI-QSAR model¹ that could be constructed for this training set using classic QSAR descriptors is

$$\begin{aligned} \log \text{ER}(J) = & 1.85 - 0.002 \times T_G - 0.0002 \times (\text{PSA} - 21.7)^2 - \\ & 0.0001 \times (\text{LUMO} - 111.2)^2 - 0.00001 \times (T_M - 444.7)^2 - \\ & 2.519 \times (\chi_{11} - 0.27)^2 + 0.781 \times \text{Dipole} + \\ & 0.011 \times (\text{Kappa5} - 11.23)^2 \\ N = 42, R^2 = 0.738, Q^2 = 0.621 \quad (8) \end{aligned}$$

The values of $\text{ER}(J)$ and those of the descriptors used in eq 7 are given in Table 7. The definitions of the classic QSAR descriptors in eqs 7 and 8 are given in Table 3. Once again, $\Delta \sum h(r)$ is the integrated difference of the monolayer CDFs with, and without, each of the skin penetration enhancers embedded in the monolayer.

The five points made about eq 5 by itself, and in comparison to eq 6, also generally hold regarding eq 7 and its comparison to eq 8. However, for eqs 7 and 8, the following distinctive points have been identified:

1. The MI-QSAR model given by eq 7 is relatively straightforward to interpret. $\Delta \sum h(r)$ suggests that the bigger the “holes” created in the monolayer by the penetration enhancer, the greater the value of $\text{ER}(J)$ in the same manner as seen in eq 5. The aqueous solvation free energy descriptor, FH2O, of eq 5 is replaced in eq 7 by polar surface area, PSA. However, the *interpretation* of these two QSAR

Table 7. The ER(*J*) and Descriptor Values for the MI-QSAR Model Given by eq 7

compound code #	PSA	Kappa5	ER(<i>J</i>)	$\Delta\sum h(r)$
SL-ACYCLIC-AZONE-AMIDES/HCA-1	40.54	12.25	13.62	0.935
SL-ACYCLIC-AZONE-AMIDES/HCA-2	29.54	13.19	20.80	0.949
SL-ACYCLIC-AZONE-AMIDES/HCA-3	38.77	12.96	20.02	1.047
SL-ACYCLIC-AZONE-AMIDES/HCA-4	40.54	12.76	25.78	1.336
SL-ACYCLIC-AZONE-AMIDES/HCA-5	29.54	13.77	35.22	1.537
SL-ACYCLIC-AZONE-AMIDES/HCA-6	38.77	13.19	24.53	1.203
SL-ACYCLIC-AZONE-AMIDES/HCA-7	66.84	14.08	14.22	1.184
SL-ACYCLIC-AZONE-AMIDES/HCA-8	77.84	14.37	5.67	0.726
SL-ACYCLIC-AZONE-AMIDES/HCA-9	37.38	11.22	5.87	0.531
SL-ACYCLIC-AZONE-AMIDES/HCA-10	37.38	11.52	14.24	0.594
SL-ACYCLIC-AZONE-AMIDES/HCA-11	29.1	13.29	57.38	1.833
SL-ACYCLIC-AZONE-AMIDES/HCA-12	29.1	15.08	29.38	1.48
SL-ACYCLIC-AZONE-AMIDES/HCA-13	38.33	13.94	6.51	1.033
SL-ACYCLIC-AZONE-AMIDES/HCA-14	60.77	12.49	10.02	1.285
SL-AZONE-AMINES/HCA-1	32.26	15.08	11.80	0.86
SL-AZONE-AMINES/HCA-2	21.26	16	16.00	0.891
SL-AZONE-AMINES/HCA-3	30.49	14.22	13.18	0.966
SL-AZONE-AMINES/HCA-4	23.47	13.29	9.16	0.8
SL-AZONE-AMINES/HCA-5	12.47	14.22	30.89	1.107
SL-AZONE-AMINES/HCA-6	21.7	13.39	8.04	0.672
SL-AZONE-AMINES/HCA-7	3.24	7.86	17.80	0.357
SL-AZONE-AMINES/HCA-8	3.24	8.69	9.87	0.308
SL-AZONE-AMINES/HCA-9	3.24	9.6	15.33	0.415
SL-AZONE-AMINES/HCA-10	12.47	9.6	25.56	0.82
SL-AZONE-AMINES/HCA-11	43.7	14.22	16.11	1.055
SL-AZONE-AMINES/HCA-12	12.36	14	13.84	0.743
SL-AZONE-THIO-AMIDE/HCA-3	35.33	7.93	13.71	0.902
SL-AZONE-THIO-AMIDE/HCA-4	35.33	8.71	8.56	0.785
SL-AZONE-THIO-AMIDE/HCA-5	35.33	9.56	4.33	0.493
SL-AZONE-THIO-AMIDE/HCA-7	20.31	9.56	34.02	1.25
SL-AZONE-THIO-AMIDE/HCA-8	44.56	8.71	2.09	0.355
SL-AZONE-THIO-AMIDE/HCA-9	35.33	9.56	7.56	0.399
SL-AZONE/HCA-3	46.61	8.15	7.09	0.503
SL-AZONE/HCA-4	46.61	9.69	5.20	0.627
SL-AZONE/HCA-5	46.61	8	44.96	1.244
SL-AZONE/HCA-6	46.61	9.59	12.67	0.874
SL-AZONE/HCA-7	46.61	8.15	10.20	0.805
SL-AZONE/HCA-8	46.61	9.69	14.07	0.891
SL-AZONE/HCA-9	37.38	7.37	18.80	0.76
SL-AZONE/HCA-10	37.38	7.37	12.24	0.655
SL-AZONE/HCA-11	37.38	8.89	14.38	0.673
SL-AZONE/HCA-12	37.38	10.46	20.00	0.92

descriptors is basically the same. As PSA increases, which corresponds to increased aqueous solubility, skin penetration enhancement decreases. The most significant difference between eqs 5 and 7 is the replacement of the Dipole descriptor in eq 5 with Kappa5, a molecular connectivity shape descriptor. It is not at all clear why there is a need to replace a polar and electrostatic descriptor (Dipole) for modeling training set 1 with a shape descriptor which, in particular, captures molecular branching within a molecule (Kappa5) for training set 2. But both the Dipole and Kappa5 descriptors are inversely related to ER(*J*), so the lower their values, the better is the penetration enhancement. One possible interpretation of these inverse relationships is that both high branching and a large dipole moment may make it more difficult for the enhancer to get fully into the membrane bilayer. Presumably, if the penetration enhancer is not integrated into the bilayer, it cannot fully exert its penetration enhancement potential.

2. Equation 7, with only three linear descriptor terms, is more significant, as judged by R^2 and Q^2 , than eq 8, which has seven descriptor terms, five of which are quadratic.

3. Since eqs 7 and 8 both contain PSA and Kappa5 as descriptors, it is reasonable to suggest that the descriptors

T_G , LUMO, T_M , Chi11, and Dipole of the classic QSAR model are all needed to capture the information residing in the MI-QSAR descriptor $\Delta\sum h(r)$ of eq 7.

The results of the random scrambling and test set validation studies for the MI-QSAR models of both training sets are given in Table 5. The random scrambling studies lead to models with average R^2 values of about 0.23 and 0.29, respectively, for training sets 1 and 2. The corresponding R^2 values of the optimum MI-QSAR models, namely, eqs 5 and 7, for the two training sets are 0.731 and 0.788, respectively. Thus, the random scrambling studies suggest that the MI-QSAR models are significant and not the result of chance correlations.

The test set validation studies indicate that test training set models constructed from random samplings, using 85% of the compounds from the original training sets, are quite comparable in both R^2 and Q^2 to the optimum models developed for their respective training sets (eqs 5 and 7). Moreover, the ability to build consistent models across subsets of the two original training sets suggests that all of these models are stable and robust with respect to the range of the chemistry sampled in each of the individual training sets.

Finally, the average R^2 of prediction across the test set compounds using the MI-QSAR models built from the original two training sets is consistently about 6–11% less than the corresponding R^2 of the MI-QSAR models. This finding is indicative of stable and meaningfully predictive models.

DISCUSSION

The most significant finding from this study is that the difference in the integrated CDF of the monolayer model, in and out of the presence of the skin penetration enhancer, $\Delta\sum h(r)$, is the dominant descriptor in the optimized MI-QSAR models of both training sets studied. Not only does this descriptor dominate the MI-QSAR models but it greatly reduces the size and complexity of these QSAR models as compared to those developed using classic intramolecular descriptors derived solely from the penetration enhancers. The MI-QSAR models with $\Delta\sum h(r)$ are very simple, as well as intuitively acceptable for the action of nonpolar skin penetration enhancers.

Overall, the MI-QSAR models indicate that good nonpolar penetration enhancers make bigger “holes” in the monolayer [$\Delta\sum h(r)$] and are less aqueous-soluble, so as to preferentially enter the monolayer, than are poor nonpolar penetration enhancers. The one nonobvious aspect of the MI-QSAR models for the two training sets is the presence of a negative Dipole descriptor term in training set 1 for HC as the reference penetrant and a negative Kappa5 descriptor term in training set 2 for HCA as the reference penetrant. As noted above, both high-branching (Kappa 5) and a large dipole moment (Dipole) may make it difficult for the enhancer to get fully into the membrane bilayer. And if the penetration enhancer is not integrated into the bilayer, it may not be able to fully exert its penetration enhancement potential. Moreover, these two descriptors are the least significant in their respective MI-QSAR models and also result from specific peculiarities, like very high branching or large dipole moments, of specific compounds in each of the two training sets.

The skin penetration enhancers of both training sets are lipidlike (and surfactant-like) in shape and take up preferred positions in the monolayer, as shown in Figure 3. In essence, the skin penetration enhancers act as surrogate DMPC molecules in the monolayer. Consequently, the bigger “holes” in the monolayer due to a skin penetration enhancer arise in two major ways. First, steric “bumps” on the skin penetration enhancer, due to, for example, structure branching as seen for the SL-ACYCLIC-AZONE-AMIDES in Table 2, can induce “holes”. But more importantly, adverse electrostatic interactions involving head groups on the skin penetration enhancers with the DMPC head groups leads to the formation of “pores” and “holes” in the monolayer.

The changes in the structure of the DMPC monolayer due to the uptake of a skin penetration enhancer have been referred to above as making “pores” and “holes” in the monolayer. The reason for using quotes around *holes* and *pores* is that these terms provide a simplistic and static view of what is actually going on in the monolayer, which is captured by $\Delta\sum h(r)$. The skin penetration enhancer is altering the structure and organization of the monolayer, which, in turn, is changing with time. At one given time, a

specific, relatively large pore may open up, which is lost at a later time. A large number of small “holes” may be created, on average, for one type of skin penetration enhancer, while another enhancer may have the effect of producing a few relatively large “holes” in the monolayer. The $\Delta\sum h(r)$ descriptor captures all of these structural variants over time and presents a time and space averaged representation of the influence of each embedded skin penetration enhancer upon both the structure and dynamics of the monolayer.

The skin penetration enhancer MI-QSAR models contain only one intermolecular MI-QSAR descriptor, namely, $\Delta\sum h(r)$, with none of the other MI-QSAR descriptors reported in Table 4 being found to be significant. However, some of the descriptors in Table 4 have been found to be very important in MI-QSAR models for other adsorption, distribution, metabolism, excretion, and toxicity (ADMET) end points, such as for eye irritation^{17,18} and caco-2 cell permeation.³ $\Delta\sum h(r)$ was not available as a trial descriptor in these earlier ADMET MI-QSAR studies. Hence, it may be worthwhile to include $\Delta\sum h(r)$ in the trial descriptor pool and to rebuild the MI-QSAR models for these training sets to see if the resultant optimized models include this descriptor and are also of a simplified form like that found in eqs 5 and 7.

ACKNOWLEDGMENT

This work was funded by the National Institutes of Health through the NIH Roadmap for Medical Research, Grant 1 R21 GM075775. Information on Novel Preclinical Tools for Predictive ADME-Toxicology can be found at <http://grants.nih.gov/grants/guide/rfa-files/RFA-RM-04-023.html>. Links to nine initiatives are found at <http://nihroadmap.nih.gov/initiatives.asp>. This work was also supported by Avon Products, Inc. Resources of The Chem21 Group, Inc. were used in performing these studies. We are grateful to Tony Hopfinger, Jr. for his assistance in the editing and proofreading of this manuscript.

REFERENCES AND NOTES

- (1) Iyer, M.; Zheng, T.; Hopfinger, A. J.; Tseng, Y. J. QSAR analyses of skin penetration enhancers. *J. Chem. Inf. Model.* **2007**, *47*, 1130–1141.
- (2) Iyer, M.; Mishra, R.; Han, Y.; Hopfinger, A. J. Predicting blood-brain barrier partitioning of organic molecules using membrane-interaction QSAR analysis. *Pharm. Res.* **2002**, *19*, 1611–1621.
- (3) Kulkarni, A.; Han, Y.; Hopfinger, A. J. Predicting Caco-2 cell permeation coefficients of organic molecules using membrane-interaction QSAR analysis. *J. Chem. Inf. Comput. Sci.* **2002**, *42*, 331–342.
- (4) Barry, B. Mode of action of penetration enhancers in human skin. *J. Controlled Release* **1987**, *6*, 85–97.
- (5) Kim, N.; El-Kattan, A.; Asbill, C. S.; Kennette, R. J.; Sowell, J. W.; Latour, R.; Michniak, B. B. Evaluation of derivatives of 3-(2-oxo-1-pyrrolidine) hexahydro-1H-azepine-2-one as dermal penetration enhancers: side chain length variation and molecular modeling. *J. Controlled Release* **2001**, *73*, 183–196.
- (6) Kanikkannar, N.; Kandimalla, K.; Lamba, S. S.; Singh, M. Structure-activity relationships of chemical penetration enhancers in transdermal drug delivery. *Curr. Med. Chem.* **1999**, *6*, 593–608.
- (7) Michniak, B. B.; Player, M. R.; Godwin, D. A.; Phillips, C. A.; Sowell, J. W., Sr. Investigation of enhancer structure activity relationships in congeners of 2-(1-Nonyl)-1,3-dioxolane. *Drug Delivery* **1995**, *2*, 117–122.
- (8) Michniak, B. B.; Player, M. R.; Godwin, D. A.; Lockhart, C. C.; Sowell, J. W., Sr. In vitro evaluation of a series of azone analogs as dermal penetration enhancers: V. miscellaneous compounds. *Int. J. Pharm.* **1998**, *161*, 169–178.
- (9) Fuhrman, L. C., Jr.; Michniak, B. B.; Behl, C. R.; Malick, A. W. Effect of novel penetration enhancers on the transdermal delivery of

- hydrocortisone: an in vitro species comparison. *J. Controlled Release* **1997**, 45, 199–206.
- (10) Godwin, D. A.; Player, M. R.; Sowell, J. W.; Michniak, B. B. Synthesis and investigation of urea compounds as transdermal penetration enhancers. *Int. J. Pharm.* **1998**, 167, 165–175.
- (11) Godwin, D. A.; Michniak, B. B. Influence of drug lipophilicity on terpenes as transdermal penetration enhancers. *Drug Dev. Ind. Pharm.* **1999**, 25 (8), 905–915.
- (12) Michniak, B. B.; Player, M. R.; Sowell, J. W., Sr. Synthesis and in vitro transdermal penetration enhancing activity of lactam n-acetic acid esters. *J. Pharm. Sci.* **1996**, 85 (2), 150–154.
- (13) Michniak, B. B.; Player, M. R.; Godwin, D. A.; Phillips, C. A.; Sowell, J. W., Sr. In vitro evaluation of a series of azone analogs as dermal penetration enhancers: IV. amines. *Int. J. Pharm.* **1995**, 116, 201–209.
- (14) Michniak, B. B.; Player, M. R.; Fuhrman, L. C.; Christensen, C. A.; Chapman, J. M.; Sowell, J. W. In vitro evaluation of a series of azone analogs as dermal penetration enhancers: II. (thio)amides. *Int. J. Pharm.* **1993**, 94, 203–210.
- (15) Michniak, B. B.; Player, M. R.; Fuhrman, L. C.; Christensen, C. A.; Chapman, J. M., Jr.; Sowell, J. W., Sr. In vitro evaluation of a series of azone analogs as dermal penetration enhancers: III. acyclic amides. *Int. J. Pharm.* **1994**, 110, 231–239.
- (16) Michniak, B. B.; Player, M. R.; Chapman, J. M.; Sowell, J. W. In vitro evaluation of a series of azone analogs as dermal penetration enhancers: I. *Int. J. Pharm.* **1993**, 91, 85–93.
- (17) Kulkarni, A. S.; Hopfinger, A. J. Membrane-interaction QSAR analysis: application to the estimation of eye irritation by organic compounds. *Pharm. Res.* **1999**, 16, 1244–1252.
- (18) Kulkarni, A. S.; Hopfinger, A. J.; Osborne, R.; Bruner, L. H.; Thompson, E. D. Prediction of Eye Irritation from Organic Chemicals Using Membrane-Interaction QSAR Analysis. *Toxicol. Sci.* **2001**, 59, 335–345.
- (19) *ADMET/MI-QSAR, version 2.2 User's Guide*; The Chem21 Group, Inc.: Lake Forest, IL, 2004.
- (20) Hauser, H.; Pascher, I.; Pearson, R. H.; Sundell, S. Preferred conformation and molecular packing of phosphatidylethanolamine and phosphatidylcholine. *Biochim. Biophys. Acta* **1981**, 650, 21–51.
- (21) *Hyperchem Release 4.5 for MS Windows*; Hypercube Inc, Waterloo: Ontario, 1998.
- (22) *Mopac*, version 6.0; Frank J. Seiler Research laboratory, United States Air Force Academy: Colorado Springs, CO.
- (23) Doherty, D. C. *Molsim Version 3.4 User's Guide*; The Chem21 Group, Inc.: Lake Forest, IL, 2005.
- (24) Berendsen, H. J. C.; Postman, J. P. M.; Gunsteren, W. F.; Nola, A. D.; Haak, J. R. Molecular dynamics with coupling to an external bath. *J. Chem. Phys.* **1984**, 81, 3684–3690.
- (25) Radial distribution function. http://en.wikipedia.org/wiki/Radial_distribution_function (accessed Jun 23, 2007).
- (26) Liu, J.; Yang, L. Effect of cholesterol on DMPC phospholipid membranes and QSAR model construction in membrane-interaction QSAR study through molecular dynamics simulation. *Biol. Med. Chem.* **2006**, 14, 2225–2234.
- (27) Rogers, D.; Hopfinger, A. J. Applications of genetic function approximation to quantitative structure-activity relationships and quantitative structure-property relationships. *J. Chem. Inf. Comput. Sci.* **1994**, 34, 854–866.
- (28) Rogers, D. *WOLF 6.2 GFA Program*; Molecular Simulation Inc.: San Diego, CA, 1994.
- (29) Friedman, J. *MultiVariate Adaptive Regression Splines*; Stanford University: Stanford, CA, 1988.

CI8000277